Ultrasonics 80 (2017) 72–77

Contents lists available at ScienceDirect

Ultrasonics

journal homepage: www.elsevier.com/locate/ultras

A differential optical interferometer for measuring short pulses of surface acoustic waves

Anurupa Shaw *, Damien Teyssieux, Vincent Laude

Institut FEMTO-ST, UMR CNRS 6174, Université Bourgogne Franche-Comté, 15B avenue des Montboucons, 25030 Besançon, France

ARTICLE INFO

Article history:
Received 16 January 2017
Received in revised form 25 April 2017
Accepted 30 April 2017
Available online 10 May 2017

Keywords:
SAW
Differential interferometer
Short acoustic pulse

ABSTRACT

The measurement of the displacements caused by the propagation of a short pulse of surface acoustic waves on a solid substrate is investigated. A stabilized time-domain differential interferometer is proposed, with the surface acoustic wave (SAW) sample placed outside the interferometer. Experiments are conducted with surface acoustic waves excited by a chirped interdigital transducer on a piezoelectric lithium niobate substrate having an operational bandwidth covering the 200–400 MHz frequency range and producing 10-ns pulses with 36 nm maximum out-of-plane displacement. The interferometric response is compared with a direct electrical measurement obtained with a receiving wide bandwidth interdigital transducer and good correspondence is observed. The effects of varying the path difference of the interferometer and the measurement position on the surface are discussed. Pulse compression along the chirped interdigital transducer is observed experimentally.

1. Introduction

Generation of intense short pulses of surface acoustic waves (SAW), either from the absorption of a short laser light pulse or from piezoelectric transduction, has important potential applications. In addition to surface phonon generation [1] and non destructive evaluation [2], it could for instance be used for acoustic soliton generation, higher harmonics generation, and more generally nonlinear acoustical signal processing. Indeed, the mechanical energy transported by SAW is strongly confined at the surface, causing a high density of elastic energy and induced strain in the supporting material. As a result, even a modest initial acoustic power could in principle be capable of inducing substantial nonlinear effects, especially if combined with pulse compression techniques similar to those used to achieve intense ultrashort laser light pulses using the chirped-pulse amplification (CPA) technique [3]. As a pre-requisite, it is needed to develop the measurement of short SAW pulses in the time domain.

Optical interferometry is a well-known technique for studying wave propagation and is often preferred over other methods for its high precision in studying wave profiles, amplitude and phase variations, standing wave patterns, or group delays [4]. Various interferometers have been developed and employed to study the ultrasonic motion of SAW. Both the Michelson interferometer depicted in Fig. 1(a) and the Sagnac interferometer depicted in Fig. 1(b) rely on the principle of interference between divided wavefronts. In both case, the SAW device or substrate supporting SAW propagation is placed within the interferometer. The Michelson interferometer compares an optical wavefront reflected on the vibrating specimen with a reference wavefront. It allows one for high resolution measurements but is extremely sensitive to fluctuations in path difference, causing a slow drift of the response over time. Various active stabilization methods [5–7] and heterodyne techniques [8–12] have been proposed to overcome this problem. In contrast, the Sagnac interferometer compares two time-delayed wavefronts that have traveled the same path of micro-optical elements, but in opposite directions. It is naturally immune to slow fluctuations in the lengths of the arms of the interferometer. It has been used for the selective detection of time-harmonic SAW propagation [13], but also for the detection of laser-generated ultrasonic short pulses [14,15]. One practical difficulty, however, is to manage the beam size difference that appears between the two different paths, as a result of focusing on the sample within the Sagnac loop [15].

The Sagnac interferometer belongs to the more general class of differential interferometers, whereby a wavefront is compared with its replica shifted either in space or time. As discussed by Monchalin [4], various differential interferometric techniques have been proposed to detect and measure surface vibrations. For example, Turner and Claus used lateral-shearing interferometry to measure the amplitude and direction of propagation of

* Corresponding author.
E-mail address: shaw.anurupa@gmail.com (A. Shaw).

http://dx.doi.org/10.1016/j.ultras.2017.04.016
0041-624X/

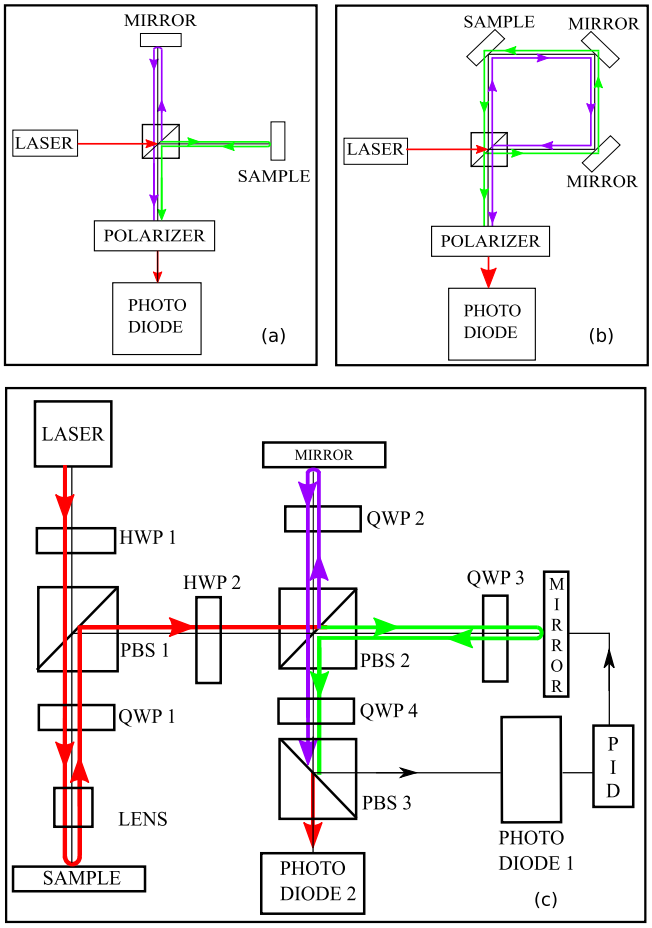

Fig. 1. Schematic representation of three optical interferometers for the measurement of surface acoustic wave short pulses. (a) Michelson interferometer with the vibrating sample inside one arm of the interferometer. (b) Sagnac interferometer with the vibrating sample inside the loop. (c) Time-shearing, or time-delay, differential interferometer with the vibrating sample before the interferometer. PBS: polarizing beam splitter, HWP: half wave plate, QWP: quarter wave plate, PID: proportional-integral-derivative controller.

ultrasonic surface waves [16]. Such measurements are suited for time-harmonic waves.

In this paper, we propose a time-delay differential interferometer in which the sample supporting SAW propagation is placed before and outside the interferometer. As a result, it allows stable maneuvering of the sample, reducing irregular overlap between the incident and reflected beams that might cause a loss in amplitude and then measurement inaccuracies. However, unlike the Sagnac interferometer, it is not immune to slow fluctuations in the differential path length and it has to be stabilized using a pro portional-integral-derivative (PID) controller. Using this setup, we investigate the measurement of short SAW pulses, with smallest durations of about 10 ns, generated by a chirped wideband interdigital transducer. In Section 2, we describe the working principle of the differential interferometer and present a mathematical analysis of the interferometric measurement. The results of an experiment devised to measure and analyze the operation of this interferometer, are discussed in Section 3, and an overall summary is provided in Section 4.

2. Working principle of the differential interferometer

The differential interferometer we have developed is depicted in Fig. 1(c). The interferometer setup is an extended version of a homodyne Michelson interferometer implementing time-shearing. A single-mode narrow-linewidth diode laser (New Focus, model Velocity 6305) with a wavelength of 651 nm and a nominal power of 7.4 mW is used as a highly coherent light source. The coherence length of the laser exceeds several hundred meters and was not a limitation in our experiments. A half-wave plate (HWP1) is placed before a polarizing beam splitter (PBS1) to adjust the input polarization. The beam is first transmitted to the sample, reflects on it, and enters the interferometric part of the setup after reflection inside PBS1. A quarter-wave plate (QWP1) provides the required polarization rotations. Four mirrors and a reflected light objective (Olympus, ultra long working distance model MSPlan 100×) are used to provide an extended path to the laser beam such that the SAW device can be placed horizontal to the optical table and the incident beam is normal to the SAW device. The spot size on the sample surface is smaller than 2 μm. This value must remain significantly smaller than the SAW wavelength in order to resolve pulse propagation. Note that after double pass through the objective the ellipticity of the laser beam is mostly corrected and the beam size inside the interferometer is about 1 mm. HWP2 and PBS2 split the laser beam into two beams of equal intensity and orthogonal polarization in the interferometer. At the exit of the interferometer, the two orthogonally polarized beams are recombined with a quarter-wave plate (QWP4) and a polarizing beam splitter (PBS3) to provide two outputs. The interference signal detected by photodiode 1 (Electro-Optics Technology, Silicon pin detector ET-2020) is used to actively stabilize the path length difference to a single quadrature point using a propor tional-integral-derivative (PID) controller for the position of one of the mirrors. The position of the mirror is controlled by a piezoelectric actuator (Thorlabs, model KC1-PZ/M, ±4 μm linear travel range) receiving the correction signal. Since the SAW signal varies on a time-scale that is much shorter than the PID response time, it remains decoupled from the correction signal. The interference signal detected by photodiode 2 (Thorlabs model DET10A/M, 1 ns rise time) provides the SAW measurement.

The output intensity on photodiode 2 after recombining the wavefronts exiting the two arms of the interferometer is

$$I(t) = I_1 + I_2 + 2m\sqrt{I_1 I_2}\cos(\phi_2(t) - \phi_1(t)) \tag{1}$$

with I_i and ϕ_i the intensity and phase in arm i. The visibility m, a number between 0 and 1, is introduced to account for possible reduction of the interference intensity because of loss of either spatial or temporal coherence. The interferometer is operated so that $I_1 \approx I_2$ to maximize interference visibility. The phase variation in either arm can be decomposed as

$$\phi_i(t) = \Phi_i + \frac{4\pi}{\lambda}u(x, t - L_i/c) + \psi_i(t) \tag{2}$$

with Φ_i a static configuration phase, independent of time, the vibration-induced deterministic phase $\frac{4\pi}{\lambda}u(t - L_i/c)$ where $u(x,t)$ is the displacement at position x that is to be measured, and $\psi_i(t)$ a random phase including all fluctuations. L_i is the optical path length of arm i, so L_i/c measures the wavefront delay, with c the speed of light. In order to provide maximum sensitivity, the stabilized interferometer is operated so that $\Phi_2 - \Phi_1 = \pi/2$ *modulo* π. Writing $\Delta u(x,t) = u(x, t - L_2/c) - u(x, t - L_1/c)$ and $\Delta\psi(t) = \psi_2(t) - \psi_1(t)$, we have

$$I(t) = I_1 + I_2 + 2m\sqrt{I_1 I_2}\sin\left(\frac{4\pi}{\lambda}\Delta u(x,t) + \Delta\psi(t)\right). \tag{3}$$

The response of the interferometer is thus nonlinear with the out-of-plane displacements $\Delta u(x,t)$. However, assuming that the displacements are small compared to the optical wavelength and that

the phase fluctuations are much less than 2π, we have approximately

$$I(t) \approx I_1 + I_2 + 2m\sqrt{I_1 I_2}\left(\frac{4\pi}{\lambda}\Delta u(x,t) + \Delta\psi(t)\right) \quad (4)$$

and the intensity changes linearly with respect to the differential displacement. The measurement depends on the path length difference $L_2 - L_1$. Indeed, we can define a delay time $\Delta t = (L_2 - L_1)/c$. If Δt is small compared to temporal variations of the displacement, then

$$\Delta u(x,t) \approx \Delta t \frac{\partial u}{\partial t}(x, t-T) \quad (5)$$

with $T = (L_2 + L_1)/2c$, and the interferometer essentially provides a measurement of the temporal derivative of the displacement. If in contrast Δt is large compared to the temporal duration of the pulse, then the same pulse will be observed twice in sequence but with a reversed sign.

The choice of the path length difference in the interferometer depends on the characteristics of the pulses to be measured. In the following section, we will present measurements for pulses with a duration $\Delta\tau$ of about 10 ns, a carrier frequency f_0 of 300 MHz, and a total bandwidth Δf of 200 MHz. First, in order for the interferometer to operate in the proportional regime, we should impose $\Delta t > \Delta\tau$, which would require $L_2 - L_1 > c\Delta\tau \approx 3$ m. In practice, this value is too large and the proportional regime would be viable only for SAW pulses typically shorter than 1 ns. Second, Eqs. (4) and (5) suggest that in the differential regime the value of Δt can be optimized. Indeed, Eq. (5) indicates that the measured intensity first increases linearly with Δt; however this increase must be limited since the range of validity of this equation is limited by the condition that Δt is small compared to temporal variations of the pulse. For a time-harmonic signal at frequency f_0, it is easily found from Eq. (4) that the optimal path length difference is given by $\Delta t = (2f_0)^{-1}$, leading to $c\Delta t \approx 0.5$ m for $f_0 = 300$ MHz. For this setting, if $u(x,t) = u_0 \sin(2\pi f_0 t)$, then $\Delta u(x,t) = 2u_0 \sin(2\pi f_0(t-T))$. For wide bandwidth signals, it should be expected that the optimal value of Δt will be slightly modified but that the order of magnitude will remain the same. This effect is discussed experimentally in the following section.

3. Results and discussion

The operation of the time-delay interferometer is evaluated using the short-pulse experiment depicted in Fig. 2. The SAW device used for this work comprise two ultra-wide bandwidth transducers. The substrate used is lithium niobate, Y+128°-rotated cut, X propagation, and the metal used for the electrodes is aluminum.

The input IDT is linearly chirped with a frequency range between 200 MHz and 400 MHz, and comprise 150 pairs of electrodes and a constant acoustic aperture of 800 μm.The acoustic aperture value is larger than 20 times the longest SAW wavelength (≈ 40 μm) and is chosen so as to reduce diffraction spreading of the SAW beam as it travels between IDTs. The distance between the input and the output IDT is 2066 μm. The output IDT is composed of only 3 electrodes and its central frequency is 300 MHz. The number of electrodes for a periodic IDT is limited by the relative bandwidth of the signal to be measured. Indeed, for a bandwidth $\Delta f = 200$ MHz and a central frequency $f_0 = 300$ MHz, the maximum number of electrode pairs N_p is calculated using [17]

$$N_p \approx \frac{f_0}{\Delta f} = \frac{300}{200} = 1.5 \quad (6)$$

With this choice, we ensure that the output IDT does not alter significantly the spectral contents of the SAW pulse and that detection is spatially localized.

An arbitrary waveform generator (AWG; Tektronix, model AWG7122B) is used to send an input chirped signal to the input IDT, through a RF high voltage amplifier (Mini-Circuits, model AN-60-008) with a voltage amplification of 40 dBm. The input chirped signal has a dispersion inverse of that of the chirped IDT, as obtained using a network analyzer. Fig. 3(a) shows the spectrum of this chirped signal. As a result of dispersion compensation, a short SAW pulse is expected to be produced on the right side of the IDT and to subsequently propagate almost unaltered on the substrate surface. On the left side of the IDT, conversely, the SAW pulse is expected to be extended in time by twice the dispersion introduced by the IDT.

The SAW pulse is detected either using the output IDT or using the time-delay interferometer, with the laser beam focused at an arbitrary point on the surface. The interferometer output is amplified using an RF amplifier (Mini-Circuits, model ZFL-1000+) with a 17 dB gain. Both the electrical and interferometer outputs are measured using an oscilloscope with a 2 GHz bandwidth, 40 GSa/s sample rate and waveform averaging value of 1024 (Agilent, model Infiniium DSO80204B).

The shortest pulse that could be observable with this system is easily obtained from the signal generated by the AWG. Indeed, for a given spectrum the shortest pulse is obtained for a constant spectral phase, i.e. in the absence of dispersion. Taking the inverse Fourier transform of the spectrum in Fig. 3(a), the 10-ns pulse shown in Fig. 3(b) is obtained. This theoretical pulse is used as a reference for experimental measurements.

The output IDT provides a differential electrical measurement of the strain field accompanying the propagation of the surface acoustic wave. More precisely, it converts the electrical charges appearing at the metal/piezoelectric interfaces into a time-dependent voltage. The strain can be assumed to be proportional to the out-of-plane displacement $u(x,t)$. As the pitch – the distance separating adjacent electrode centers – is equal to half the acoustic wavelength at a frequency of 300 MHz and since the electrodes are alternated, the voltage that is measured can be approximated as

$$V(t) = Z_0 e_{\text{eff}} \frac{\partial u(x_0,t)}{\partial t} \quad (7)$$

with Z_0 the IDT impedance, e_{eff} an effective piezoelectric coefficient expressed in C/m, and x_0 the central position of the output IDT. From Eqs. (4)–(7), it is apparent that the electrical and the optical measurements should be proportional in case the delay Δt is small.

The amplified electrical and interferometer measurements at the output electrodes are compared in Fig. 4. The amplification used to obtain both measurements are different and hence both responses are normalized independently. For both measurements, the overall shape of the waveform is conserved and is in good agreement with the theoretical pulse shown in Fig. 3(b). However, it is observed that the main pulse is followed by consecutive ripples with diminishing amplitude. We attribute that to electronic reflections resulting from impedance mismatch between the sample and the input electrical circuitry. The signal-to-noise ratio for the interferometric measurement is close to 900, while that of the electrical measurement is close to 9000. As a result the optical detection is about 10 times less sensitive than the electrical detection. However, optical detection can be performed at an arbitrary location on the surface of the sample, while electrical detection is only possible at the location of the output IDT. Furthermore, electrical detection involves integration along all the acoustic aperture, or 800 μm, while optical detection is performed at the laser focus, within an area smaller than 4 μm^2. Possible directions of improvement include optimizing the optical power loss in the

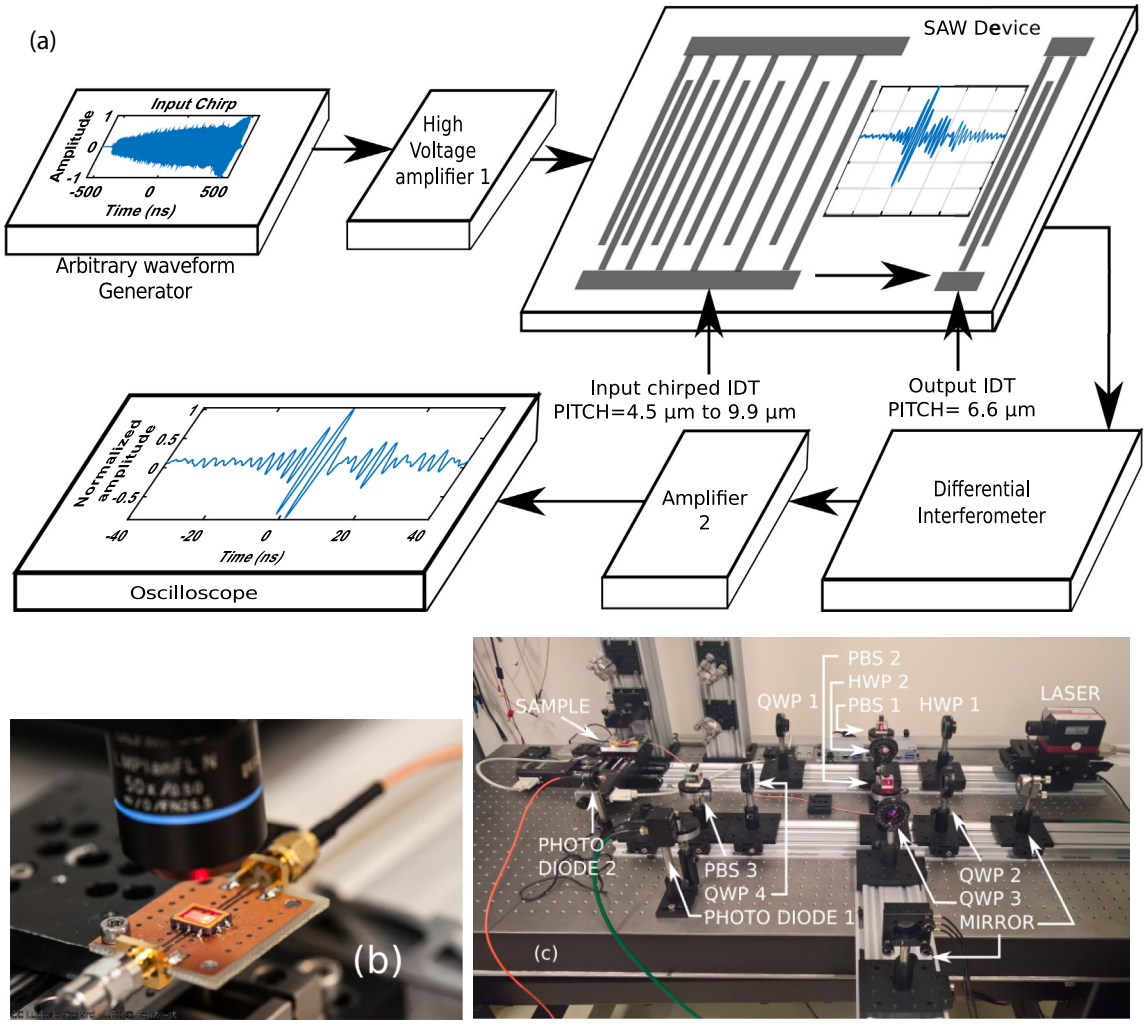

Fig. 2. (a) Schematic of the short-pulse surface acoustic wave experiment. IDT: interdigital transducer. (b) Close view at the sample mounting. (c) Photograph of the differential interferometer setup with elements indicated following the schematic in Fig. 1(c).

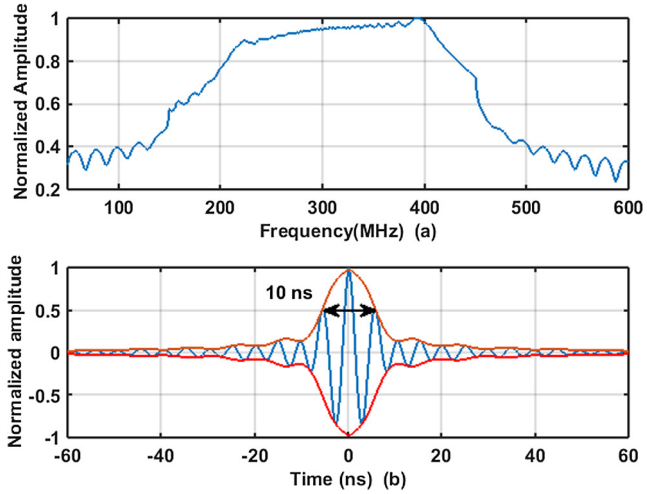

Fig. 3. (a) Spectrum of the input chirp signal generated by the arbitrary waveform generator. (b) Theoretical shortest pulse, as obtained by Fourier transforming the spectrum of the input chirp signal assuming constant spectral phase. The full-width at half-maximum (FWHM) is 10 ns.

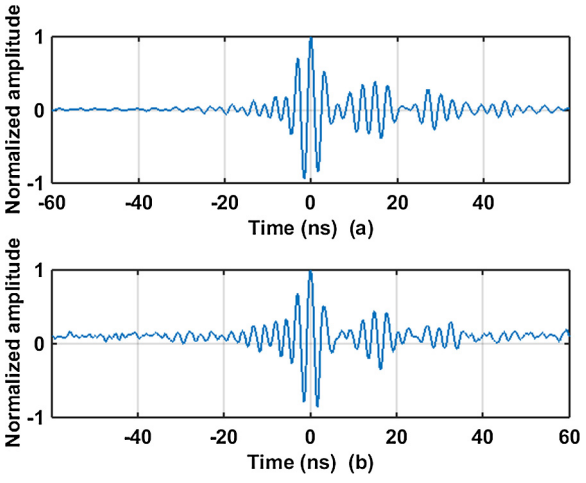

Fig. 4. Electrical measurement (a) and interferometer measurement (b) at the location of the output interdigital transducer.

setup. For the measurements that are presented, the optical beams suffer a 55.8% amplitude loss. Other possible improvements include correction of slight misalignment of the optical components and polarization of laser beams, and compensation of slight differences in the width of the beams passing through the objective.

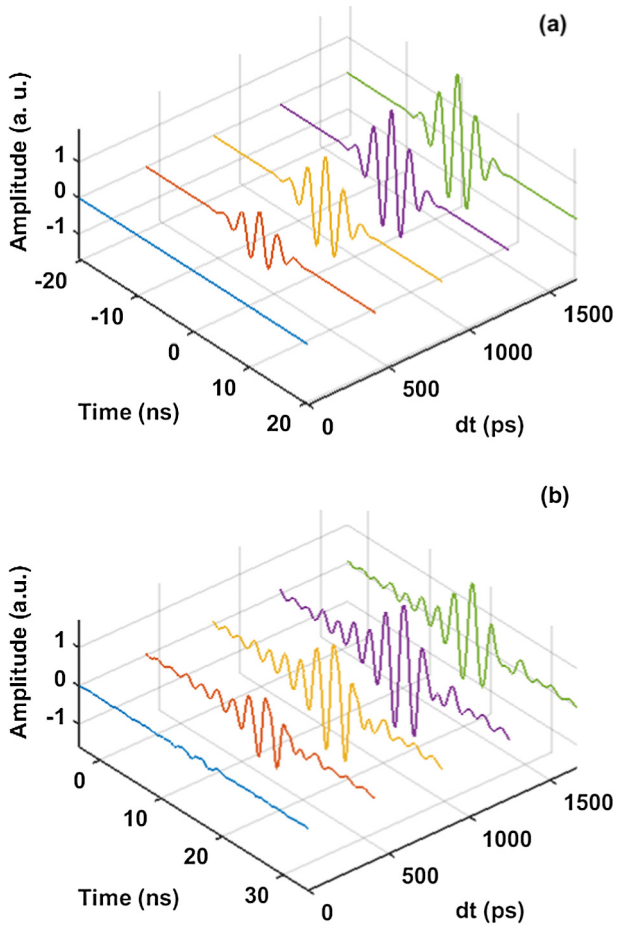

Fig. 5. Dependence of the pulse measurement with the time-delay Δt. (a) Plot of $\Delta u(x,t)$ at a given position as a function of Δt, for a 10-ns Gaussian pulse. (b) Experimental result as a function of Δt obtained by changing the path length difference in the interferometer.

Time-delay operation was further checked by repeating the interferometric measurement for different values of the path length difference $L_2 - L_1 = c\Delta t$. The results are presented in Fig. 5 and compared with Eq. (4) using the theoretical pulse of Fig. 3 (b). The experimental result is found to be consistent with the theoretical result and shows that the dynamic response of the interferometer can be adjusted depending on the duration of the pulse that is to be measured. For the central 300 MHz frequency that is used here, the path length difference giving the optical measurement was found to be around 30 cm. Clearly, this distance would be reduced in proportion for shorter pulses, i.e. larger SAW carrier frequencies. For this optimal path length difference, we estimated the maximum amplitude of the surface displacements as follows. The total voltage output was first calibrated with the PID off by sweeping the moving mirror position over a path length difference larger than one optical wavelength. Switching the PID on, it was then determined that the measurement scale in Fig. 5 converts to a full range of 36 nm. The actual detection limit was further determined from the root-mean-square (rms) noise value obtained with the PID on but with the SAW signal off. Conversion to amplitude vibration gives a value of 40 pm for the detection limit.

Interferometric measurements were repeated at different locations along the SAW beam path from the exit of the chirped IDT to the output IDT. It was found that the SAW pulse shape showed very little distortion as a function of position. More interestingly, measurements were performed along the chirped IDT, from the left side ($x = 0$) to the right side ($x = 1800$ μm), as shown in Fig. 6. On the left side, the SAW pulse is so dispersed that its amplitude is very low. As the measurement position is moved to the right, the compressed pulse is seen to emerge as more and more frequency components become synchronized. At the right side of the chirped IDT, all frequency components are in phase and add up to form the final 10-ns pulse.

4. Conclusion

In summary, we have described a differential interferometer that is capable of time domain shearing and provides short pulse measurement of surface acoustic waves. The interferometer is an extended version of a Michelson interferometer implementing time-shearing. It is stabilized against low frequency noise using a PID controller actively maintaining the path length difference at a single quadrature point. Short SAW pulses with a duration of 10 ns produced by an ultra-wide bandwidth chirped SAW transducer were measured and compared with an equivalent electrical

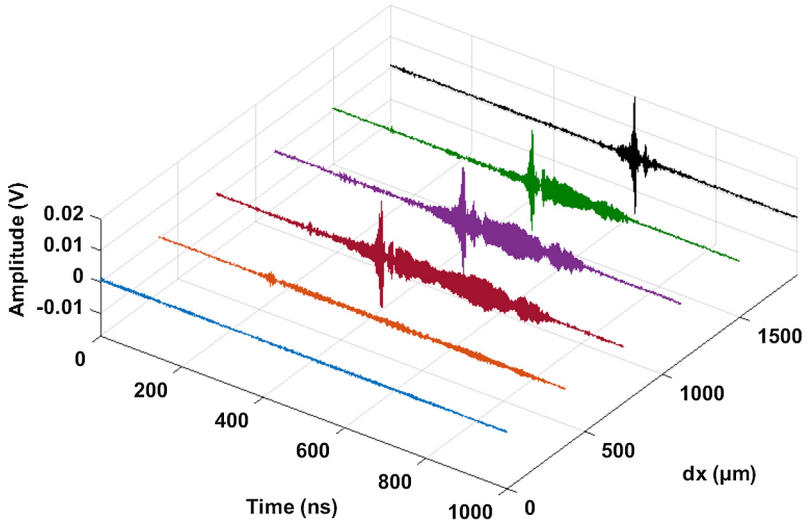

Fig. 6. Measurement of the SAW pulse at various positions along the chirped interdigital transducer. A movie of pulse compression along the chirped interdigital transducer is available as supplementary material.

measurement and with theory. Good agreement was found and the overall waveform was well conserved. Maximum displacements of about 36 nm were observed, with a detection limit of 40 pm. Pulse compression along the chirped SAW transducer was furthermore observed experimentally.

Acknowledgments

Support from the Région de Bourgogne Franche-Comté under grant 2014C-15446 is gratefully acknowledged. We wish to thank Dr. Sarah Benchabane and Dr. Jean-Michel Friedt for enlightening discussions and suggestions. Experimental help from Gilles Martin and Valérie Pétrini is gratefully acknowledged.

Appendix A. Supplementary material

Supplementary data associated with this article can be found, in the online version, at http://dx.doi.org/10.1016/j.ultras.2017.04.016.

References

[1] Y. Sugawara, O.B. Wright, O. Matsuda, M. Takigahira, Y. Tanaka, S. Tamura, V.E. Gusev, Watching ripples on crystals, Phys. Rev. Lett. 88 (18) (2002) 185504.
[2] S.J. Davies, Chris Edwards, G.S. Taylor, Stuart B. Palmer, Laser-generated ultrasound: its properties, mechanisms and multifarious applications, J. Phys. D: Appl. Phys. 26 (3) (1993) 329.
[3] Donna Strickland, Gerard Mourou, Compression of amplified chirped optical pulses, Opt. Commun. 56 (3) (1985) 219–221.
[4] J.-P. Monchalin, Optical detection of ultrasound, IEEE Trans. Ultrason., Ferroelec., Freq. Control 33 (1986) 485–499.
[5] Jouni V. Knuuttila, Pasi T. Tikka, Martti M. Salomaa, Scanning Michelson interferometer for imaging surface acoustic wave fields, Opt. Lett. 25 (9) (2000) 613–615.
[6] J.E. Graebner, B.P. Barber, P.L. Gammel, D.S. Greywall, S. Gopani, Dynamic visualization of subangstrom high-frequency surface vibrations, Appl. Phys. Lett. 78 (2) (2001) 159–161.
[7] Lauri Lipiäinen, Kimmo Kokkonen, Matti Kaivola, Phase sensitive absolute amplitude detection of surface vibrations using homodyne interferometry without active stabilization, J. Appl. Phys. 108 (11) (2010) 114510.
[8] D. Royer, O. Casula, A sensitive ultrasonics method for measuring transient motions of a surface, Appl. Phys. Lett. 67 (1995) 3248–3250.
[9] Pascal Vairac, Bernard Cretin, New structures for heterodyne interferometric probes using double-pass, Opt. Commun. 132 (1–2) (1996) 19–23.
[10] Hanne Martinussen, Astrid Aksnes, Helge E. Engan, Wide frequency range measurements of absolute phase and amplitude of vibrations in micro-and nanostructures by optical interferometry, Opt. Express 15 (18) (2007) 11370–11384.
[11] K. Kokkonen, M. Kaivola, S. Benchabane, A. Khelif, V. Laude, Scattering of surface acoustic waves by a phononic crystal revealed by heterodyne interferometry, Appl. Phys. Lett. 91 (2007) 083517.
[12] Kimmo Kokkonen, Matti Kaivola, Scanning heterodyne laser interferometer for phase-sensitive absolute-amplitude measurements of surface vibrations, Appl. Phys. Lett. 92 (6) (2008) 063502.
[13] Ken-Ya Hashimoto, Keiskue Kashiwa, Nan Wu, Tatsuya Omori, Masatsune Yamaguchi, Osamu Takano, Sakae Meguro, Koichi Akahane, A laser probe based on a sagnac interferometer with fast mechanical scan for RF surface and bulk acoustic wave devices, IEEE Trans. Ultrason., Ferroelec., Freq. Control 58 (1) (2011) 187–194.
[14] David H. Hurley, Oliver B. Wright, Detection of ultrafast phenomena by use of a modified sagnac interferometer, Opt. Lett. 24 (18) (1999) 1305–1307.
[15] Takehiro Tachizaki, Toshihiro Muroya, Osamu Matsuda, Yoshihiro Sugawara, David H. Hurley, Oliver B. Wright, Scanning ultrafast sagnac interferometry for imaging two-dimensional surface wave propagation, Rev. Sci. Instrum. 77 (4) (2006) 043713.
[16] Richard O. Claus and Tyson M. Turner, Dual differential interferometer, 1985. US Patent 4,512,661.
[17] D.P. Morgan, Surface-Wave Devices for Signal Processing, Elsevier, 1985.